ASCE

Rebuilding Syria from the Rubble: Recycled Concrete Aggregate from War-Destroyed Buildings

Abdulkader Rashwani[1]; Bakry Kadan[2]; Sepehr Seyedian Choubi[3]; Yousef Alhammoudi[4]; Theodore Hanein[5]; Maurizio Guadagnini[6]; Cagla Meral Akgul[7]; and John L. Provis[8]

Abstract: The ongoing Syrian civil war began in 2011 and has left more than 130,000 buildings destroyed, 70% of which are RC buildings. When the war is over, it is estimated that the millions of displaced refugees will return within 8 years, thus requiring a rapid urban redevelopment of the country. This study examined the feasibility of reusing concrete from destroyed buildings as recycled concrete aggregate (RCA), and will assist in developing much-needed recommendations for the sustainable redevelopment of Syria's infrastructure. Although the concept of RCA is not specifically novel, the properties of RCA generated from different sources must be assessed thoroughly to confirm its reuse potential. Never has demolished concrete been so widely available as it is now in parts of Syria, rendering the potential impact of this work enormous. In this study, simple and established methods were implemented to collect and test materials, to simulate more closely real-life scenarios of when the country's reconstruction is to start. The chemical and physical properties of the aggregate were measured, followed by the determination of fresh and hardened properties of the concrete produced using a mixture of RCA and natural aggregates. For the first time, this study provides evidence that RCA from the rubble of war-destroyed Syrian buildings can be immediately valorized as a sustainable alternative to natural coarse aggregates in concrete; up to 50% replacement can be achieved without significantly affecting the performance of the new concrete. **DOI: 10.1061/(ASCE)MT.1943-5533.0004654.**

Author keywords: Recycled concrete aggregate (RCA); Waste valorization; Syrian civil war; Concrete testing; Circular economy.

Introduction

Since March 2011, the ongoing civil war in Syria has left more than 130,000 buildings damaged or destroyed. This crisis also has resulted in an unparalleled decline in well-being, escalated the poverty rate in the country, and forcibly displaced 5.6 million people of the prewar population of 22 million (Cheung et al. 2020).

When conflict ends in Syria, people are projected to return at a rate of 12% per year, meaning that major devastated cities, from which more than half the population has emigrated, could regain their prewar population in less than 10 years (Qudsi 2017).

When the reconstruction process of Syria begins, costs and imports must be kept to a minimum. The recycling of the readily available destroyed buildings could allow for affordable reconstruction and promote repatriation. The rubble of demolished buildings is a valuable source of construction materials to be used in the same areas that require rapid rebuilding at the lowest possible cost and in the shortest amount of time. The steel rebar can be separated easily from the rubble with magnets, and either manually reused as reinforcement or sent to plants and processed into new steel. The remaining concrete can be crushed to make recycled concrete aggregate (RCA) for new concrete. It already has been shown in many regions that partial replacement of natural aggregate (NA) with recycled concrete aggregate does not affect the mechanical and durability performance of concrete (Limbachiya et al. 2000; Eguchi et al. 2007). Standards allow the use of a high percentages of RCA [up to 50%, e.g., in EN 12620:2013/EN 206:2013+A1:2016 (CEN 2013, 2016)]. However, different countries have different construction methods and raw materials; therefore, it is necessary to demonstrate the reuse of RCA obtained from different sources at a local level.

Vast amounts of RCA currently are available in some areas of Syria, such as Aleppo, where rapid reconstruction is essential to enable the repatriation of the population. The broader use of RCA also can promote the resilience and well-being of the Syrian population by creating new job opportunities and reducing building time. RCA also will enable the development of sustainable solutions in the region by promoting a circular economy in the construction industry and reducing the extraction of virgin resources. Rebuilding the country using these concepts also can support a foundation to enable the future Syria to be a technological hub for green and circular materials and construction solutions in the region.

This paper presents the methodology implemented to identify, collect, and classify RCA in specific regions of Syria and provide recommendations to enable RCA's immediate use in new concrete

[1]Assistant Professor, Dept. of Chemical Engineering, Sham Univ., Aleppo, Syria. ORCID: https://orcid.org/0000-0001-7196-880X. Email: rashwani@gmail.com

[2]Assistant Professor, Dept. of Chemical Engineering, Sham Univ., Aleppo, Syria. Email: bakreechem@gmail.com

[3]Ph.D. Student, Dept. of Civil Engineering, Middle East Technical Univ., Ankara 06800, Turkey. ORCID: https://orcid.org/0000-0002-0299-7858. Email: sepehr.seyedian@gmail.com

[4]Assistant Professor, Dept. of Chemical Engineering, Sham Univ., Aleppo, Syria. Email: eng.y.hamoudi@gmail.com

[5]UKRI Future Leaders Fellow, Dept. of Materials Science and Engineering, Univ. of Sheffield, Sheffield S1 3JD, UK. ORCID: https://orcid.org/0000-0002-3009-703X. Email: t.hanein@sheffield.ac.uk

[6]Senior Lecturer, Dept. of Civil and Structural Engineering, Univ. of Sheffield, Sheffield S1 3JD, UK. Email: m.guadagnini@sheffield.ac.uk

[7]Assistant Professor, Dept. of Civil Engineering, Middle East Technical Univ., Ankara 06800, Turkey. Email: cmeral@metu.edu.tr

[8]Professor, Dept. of Materials Science and Engineering, Univ. of Sheffield, Sheffield S1 3JD, UK (corresponding author). ORCID: https://orcid.org/0000-0003-3372-8922. Email: j.provis@sheffield.ac.uk

Note. This manuscript was submitted on December 2, 2021; approved on July 1, 2022; published online on January 18, 2023. Discussion period open until June 18, 2023; separate discussions must be submitted for individual papers. This paper is part of the ***Journal of Materials in Civil Engineering***, © ASCE, ISSN 0899-1561.

to promote rapid reconstruction of Syria's infrastructure. Possible valorization routes for the remaining parts of the rubble also are identified, and additional urgent research needs are discussed.

Materials

The coarse and fine aggregates used in this study are shown in Fig. 1. The natural aggregate was obtained from the city of Afrin, and was a crushed limestone with a maximum nominal size of 20 mm. The fineness moduli of the natural calcium sand and fine river sand were 3.5 and 2.9, respectively. The RCAs were obtained from different sites (Fig. 2). A cement type CEM II/A-W 42.5 R [EN 197-1:2011 (CEN 2011)] was used in all mixes investigated in this comparative study.

The RCA used in this study was obtained from the rubble of destroyed buildings in Al-Bab city in northern Syria (Fig. 2). Generally, rural sites comprise buildings made of masonry concrete, whereas buildings in urban sites are made predominantly of RC.

Five urban and five rural sites were chosen to obtain representative samples of the different types of concrete used in Syria in typical buildings. In urban sites, concrete from hospitals, schools, silos, and residential and office buildings was collected, whereas in rural sites, the people store debris in open spaces, and we collected the samples from these piles. Clay, plaster, or any other foreign materials were avoided. Fig. 2 shows the location of the sites from which rubble samples were collected, and additional information is included in Table 1.

BEcause the buildings examined in this study were destroyed with weapons of unknown nature, the amount of radioactivity of the parent concrete was measured with a Radex RD1503+ (Quarta-Rad. Wilmington, Delaware) Geiger counter before collecting any samples, ensuring safety for personnel and in material reuse [Fig. 3(a)]. The radioactivity level measured at all sites ranged between 0.10 and 0.13 μSv/h, corresponding to a permissible value. An initial assessment of the parent concrete also was conducted through in situ nondestructive tests [ASTM C805/C805M-1 (ASTM 2018b)] using an N-type Schmidt hammer. Although Schmidt hammer tests take readings from the surfaces exposed to weathering conditions, the readings provide a conservative lower strength limit of the parent concrete.

Approximately 1,200 kg of debris containing concrete and bricks from the chosen sites in Al-Bab city were collected by coning and quartering methods [Fig. 3(b)] to ensure proper sampling

Fig. 1. Fine and coarse aggregates used in this study: (a) RCA; (b) NA; (c) natural calcareous sand; and (d) river sand.

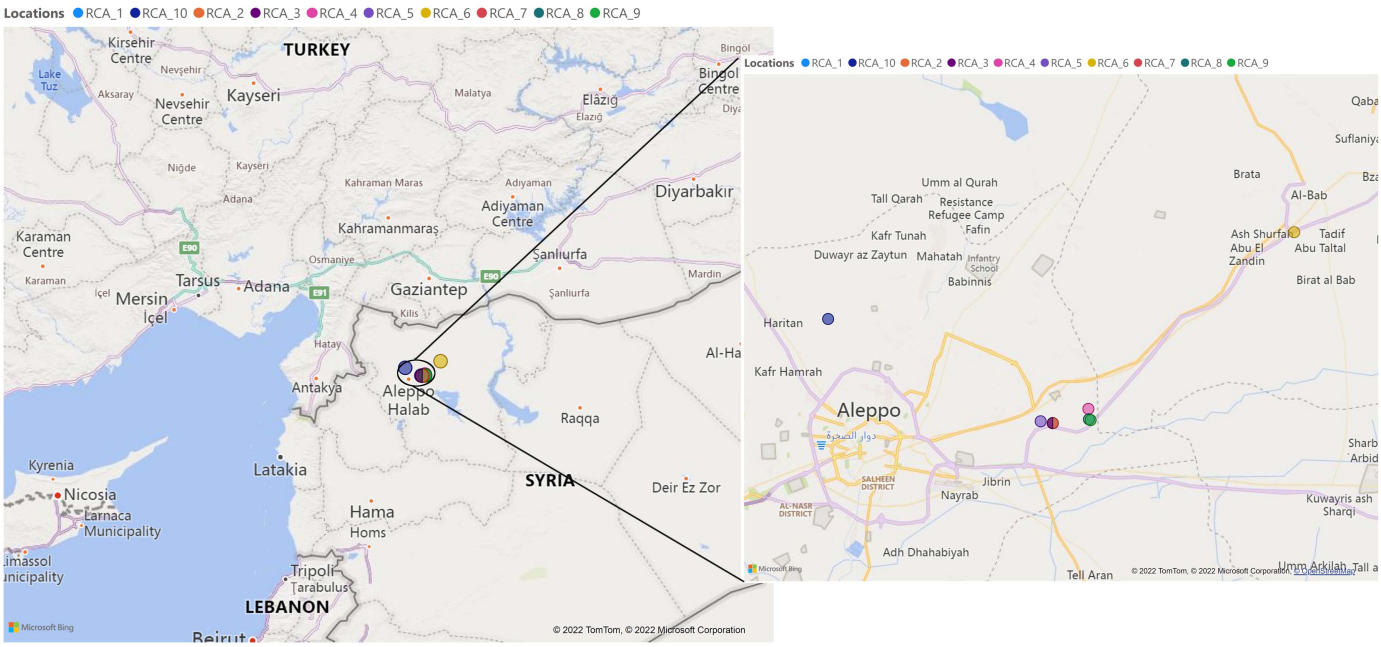

Fig. 2. Map of sites from which the samples of RCA were collected. (© 2022 TomTom, © 2022 Microsoft Corporation, © OpenStreetMap.)

Table 1. ID and characteristics of aggregates included in RCA samples collected for this study

Sample ID	Site No.	Site type	Aggregate type	Sample ID	Site No.	Site type	Aggregate type
RCA_1	1	Urban	S	RCA_6	6	Rural	S-C
RCA_2	2	Urban	S	RCA_7	7	Rural	S-C
RCA_3	3	Urban	C	RCA_8	8	Rural	S-C
RCA_4	4	Urban	S	RCA_9	9	Rural	C
RCA_5	5	Urban	S-C	RCA_10	10	Rural	C

Note: S = siliceous; S-C = siliceous-calcareous; and C = calcareous.

(a) (b) (c)

Fig. 3. Collection procedure for the RCA: (a) radiation measurements; (b) coning and quartering sampling method; and (c) crushing of concrete rubble with jaw crusher.

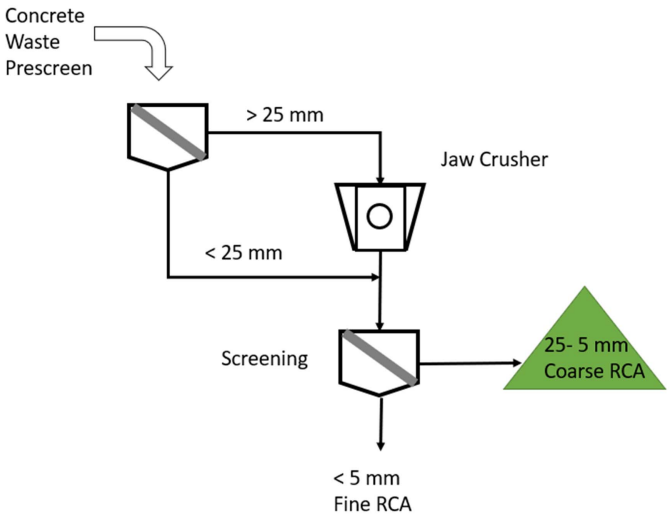

Fig. 4. Production stages of recycled concrete aggregate.

(ASTM International 2001b). Jaw crushers [Fig. 3(c)] and screens with a maximum sieve size of 25 mm were used to produce RCA in various sizes. RCA was divided further into coarse (over 5 mm), and fine (under 5 mm) aggregates. The coarse aggregate was placed on a 63-μm sieve and washed with water to remove clay impurities; finally, the RCA was dried in air.

The process of producing the RCA is shown in Fig. 4.

Characterization of RCA

The RCAs collected from the selected sites were characterized fully for physical, chemical, and mineralogical properties. The methodologies implemented to determine relevant material properties are described in the following sections.

Physical Properties

All physical properties were determined from a minimum of three specimens and are reported here in terms of average values. The particle-size distribution (PSD) was determined for all aggregate fractions according to ASTM C136 (ASTM International 2001b), whereas the dry particle density (bulk density) and water absorption were determined according to ASTM C127-01 (ASTM International 2001c). The Los Angeles degradation test was used to evaluate the resistance of the coarse recycled aggregates to possible degradation due to the effects of abrasion, wear, and impact (ASTM International 2003a).

Chemical and Mineralogical Properties

Chemical and microstructural characterization was performed through X-ray fluorescence (XRF), thermogravimetric (TG) analysis (TGA), X-ray diffraction (XRD), and scanning electron microscopy with energy dispersive spectroscopy (SEM/EDS). All XRD, TG, and XRF samples were ground to a fine powder (<63 μm) using a mortar and pestle.

The chemical analysis of the RCA samples was performed using a Malvern Panalytical (Malvern, UK) Zetium XRF instrument. A Claisse LeNeo Fluxer (Malvern, UK) was used to make beads, and the XRF measurement was conducted using Malvern Panalytical SuperQ software. Malvern Panalytical wide-ranging oxides (WROXI) calibration was used to determine the oxide concentrations in terms of percentage by weight. The fused 40-mm beads used for measurements were made by mixing 10 g lithium tetraborate (with 0.5% LiBr) flux with 1 g of sample.

The samples also were analyzed by thermogravimetric analysis coupled with mass spectrometry (TGA-MS) [Netzsch TG 449 F3 (Selb, Germany) Jupiter coupled to a mass spectrometer]. Samples

of 35 ± 0.5 mg were placed in an alumina crucible and exposed under an inert atmosphere of argon, increasing the temperature from 30°C to 1,000°C with a heating rate of 10°C/min with argon gas as the purging gas. A blank curve, obtained under the same conditions with the same empty alumina crucible, was subtracted systematically. All samples were held at 30°C for 20 min before the heating process began.

The mineralogy of the powdered samples was scanned using X-ray diffraction (Bruker D8, Billerica, Massachusetts) in the 2θ range of 5°–70° at a step size of 0.020° 2θ for 2 h, using CuKα radiation (1.5406 Å). All analyses were conducted using ground powder samples.

The surface microstructure of pellets and granules prepared from RCA was analyzed using scanning electron microscopy [Hitachi TM-3000 (Tokyo) microscope with the QUANTAX 70 program, Japan]. For microscopy, small cuboid samples were cut from the RCA specimens. Elemental compositions were investigated using an energy dispersive spectrometer in conjunction with SEM imaging.

Characterization of Concrete with RCA

Concrete mixes including different percentages of RCA replacement were examined to determine the effect of the replacement ratio on the mechanical properties and the durability of the resulting concrete. Five different concrete mixes were prepared (Table 2), including a control mix (0% replacement of NA) and four mixes with an increasing proportion of RCA replacement (25%, 50%, 75%, and 100% of NA). All concrete mixes were designed following the BR 331 (Teychenné et al. 1997) method, and a target compressive strength of 25 MPa was considered for the control mix. Because RCA typically has high water absorption (Xiao et al. 2012a, b), the RCA was presoaked in water for 24 h before mixing. A slump between 8 and 10 cm was targeted for all mixes to ensure similar workability, and the water–cement (W/C) ratio was adjusted accordingly. Superplasticizer [Aydos300 (Aydos, Dilovası, Turkey)] at a dosage of 1% of cement weight (3.62 kg/m^3) was used for all mixes.

Fresh Concrete Properties

Slump tests were performed to measure the workability of fresh concrete. The tests were carried out following ASTM C143 (ASTM International 2003b). As an indication of consistency between different batches, the slump was measured for every batch of mixes. Density measurements were taken following ASTM C138 (ASTM International 2001a).

Hardened Concrete Properties

The complementary set of tests conducted to characterize the hardened properties of the mixes is summarized in Table 3 and described in detail in this section. At least three replicate specimens were examined for each of the reported properties.

Mechanical Properties

Mechanical tests were conducted on 28-day-old samples that were moisture-cured in a mist room until the day of testing. Cylinders $\phi 150 \times 300$ mm were used to determine the compressive strength, f'_c, of all mixes (ASTM International 2018a), and $\phi 100 \times 200$-mm cylinders were used to measure elastic modulus, E, and Poisson's ratio, ν (ASTM International 2002c), and to provide additional compressive strength points (converted to equivalence with the $\phi 150 \times 300$-mm cylinders using a correction factor of 0.97). The cylinders were capped with a sulfur capping compound before testing to distribute the loading forces evenly. The cylinders used to determine E and ν were fitted with two LVDTs and one crack opening displacement (COD) gauge for measuring the longitudinal and lateral displacements, respectively. The cylinders were loaded to 40% f'_c, and the longitudinal deformations were calculated by

Table 2. Concrete mix designs

Mix ID	RCA content (% by weight)	W/C	Water (kg/m^3)	Cement (kg/m^3)	Sand[a] (kg/m^3)	NA—crushed limestone (kg/m^3)	RCA (kg/m^3)
Control	0	0.53	190	362	604	1,174	0
RCA25	25	0.53	190	362	604	880.5	293.5
RCA50	50	0.53	190	362	604	587	587
RCA75	75	0.55	200	362	604	293.5	880.5
RCA100	100	0.57	208	362	604	0	1,174

[a]Sand used comprised 15% by weight natural calcareous sand and 85% by weight river sand.

Table 3. Tests of hardened concrete

Test	Method	Specimen geometry	Specimen age
Compressive strength	ASTM C39-18	$\phi 150 \times 300$ mm	28 days
Elastic modulus and Poisson's ratio	ASTM C469-02	$\phi 100 \times 200$ mm	28 days
Splitting tensile	ASTM C496-02	$\phi 150 \times 300$ mm	28 days
Flexural strength	ASTM C293-02	$100 \times 100 \times 400$ mm	28 days
Drying shrinkage	ISO 1920-8	$100 \times 100 \times 300$ mm	Measurements start at 24 h after casting, then continue daily or every other day up to 28 days
Water permeability	BS EN 12390-8	$\phi 100 \times 200$ mm	48 days[a]
Rapid chloride ion permeability	ASTM C1202-12	$\phi 100 \times 50$ mm	48 days[a]
Rate of water absorption	ASTM C1585-13	$\phi 100 \times 50$ mm	48 days[a]
Density, absorption, and voids in hardened concrete	ASTM C642-97	Volume not less than 350 cm^3(~800 g)	48 days[a]

[a]According to the standards, the measurements do not have to be conducted precisely at 28 days.

averaging the reading from the two LVDTs. The lateral deformations were calculated to be 44% of the COD reading considering the geometry of the compressometer. The tensile strength was determined through splitting tensile testing of $\phi 150 \times 300$-mm cylinders (ASTM International 2002b), and the flexural strength was determined using $100 \times 100 \times 400$-mm prismatic specimens subjected to three-point bending (ASTM International 2002a).

Drying Shrinkage

The drying shrinkage of the concrete mixes (ISO 2009) was monitored through measurements on prismatic specimens ($100 \times 100 \times 300$ mm) using a DEMEC (Mastrad, Douglas, UK) mechanical strain gauge, starting immediately after demolding, which took place 24 h after casting. Two pairs of DEMEC discs were glued 200 mm apart on two of the longitudinal sides of each specimen (Fig. 5). The exact distance between each pair of discs was measured, and the average of the two measurements was considered to be the initial length. The distance between the DEMEC discs was monitored for up to 28 days, and the specimens were kept in a room with a constant temperature of 22°C ± 1°C and humidity of 30% for the duration of the test. For each specimen, the average percentage change in the distance between the DEMEC points was reported as the drying shrinkage.

Water Permeability

The depth of water penetration under pressure (BSI 2003) was determined on 48-day-old air-cured cylindrical specimens with dimensions of $\phi 100 \times 200$ mm. Water pressure of 500 kPa (5 bar) (equivalent to keeping the specimens at a depth of 50 m underwater) was applied to the bottom surface of the specimens for 72 h. At the end of the test, the samples were split in half perpendicular to the face on which the water pressure was applied. After the specimens were dry enough to identify the water front, the maximum depth of water penetration was measured.

Water Absorption by Capillary Rise

The durability of concrete subjected to aggressive environments depends strongly on the penetrability of the pore system (Kou and Poon 2008). Absorption by capillary rise is critical for the rate of ingress of liquids. In this paper, the one-dimensional water absorption rate in concrete specimens was measured according to Kou and Poon (2008). Discs 50 mm thick were saw-cut from 28-day old $\phi 100 \times 200$-mm cylindrical specimens. The specimens were air-cured for 20 days, and their weights were recorded each day until weight stabilization was ensured. All surfaces of the specimens not exposed to water were sealed with a waterproof band. Subsequently, the concrete discs were placed in a pan and immersed in tap water up to a level of 3 mm. The specimens were weighed at the time intervals specified in ASTM C1585 (ASTM International 2013), and the absorption was defined as the change in mass divided by the product of the exposed area and density of water. The initial and secondary rates of water absorption values were determined as the slope of the absorption versus the square root of time curves during the first 6 h and from 1 to 7 days, respectively.

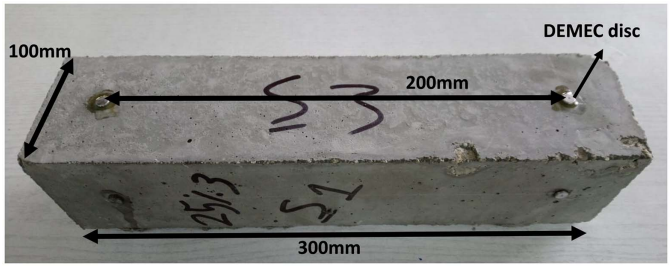

Fig. 5. Drying shrinkage specimens.

Rapid Chloride Ion Penetration

The electrical conductance of concrete is a rapid indication of its resistance to chloride-ion penetration (ASTM International 2012). In this paper, chloride ion penetration tests were carried out according to ASTM C1202 (ASTM International 2012). Discs 50 mm thick were saw-cut from 28-day-old $\phi 100 \times 200$-mm cylindrical specimens and air-cured for 20 days. The side of the discs was sealed, and the discs were vacuum-saturated using a vacuum desiccator. Subsequently, the discs were mounted into rapid chloride test (RCT) cells using rubber gaskets to prevent leakage of the solutions during the test. The NaOH (0.3 mol/L) and NaCl (3%) chambers were filled. A 60.0 ± 0.1 V voltage was applied for 6 h, and the current was recorded at least every 30 min. The total charges passed (in coulombs) were calculated from the area under the current versus time curve.

Density, Absorption, and Voids in Hardened Concrete

Specimens weighing about 1 kg were cut from the concrete prisms used in flexural strength tests. The samples were weighed under different conditions: oven-dried, saturated after immersion, saturated after boiling, and immersed underwater. The measured weights were used to determine density, absorption, and permeable void ratio according to ASTM C642 (ASTM International 1997).

Account of Findings

Compressive Strength of Parent Concrete by Schmidt Hammer

The compressive strength of parent concrete in two sites in Al-Bab city was estimated using a Schmidt hammer. Tests of structural elements including columns, beams, slabs, and stairwells resulted in concrete strengths ranging from 36 to 57 MPa, which corresponds to a concrete type 25 or higher according to the Syrian standards (Syrian Engineers Union 2006). These data are presented in Table 4.

Properties of the Recycled Concrete Aggregates

Physical Properties of Coarse Aggregates

Grain Distribution. Particle-size distribution is one of the essential properties of aggregates because it directly affects the properties of concrete, such as workability, porosity, permeability, strength, degree of compaction, and durability. A continuous PSD indicates that the aggregate is uniformly graded in all sizes, allowing greater

Table 4. Schmidt values obtained from parent concrete investigated in this study

Sample ID	Location	Average of Schmidt values, representing compressive strength (MPa)	Standard deviation
RCA_1	Malyei (1)—column	40	1.46
RCA_1	Malyei (1)—beam 1	56	4.35
RCA_1	Malyei (1)—beam 2	33	3.23
RCA_1	Malyei (1)—stairwell	57	4.51
RCA_2	Malyei (2)—column	39	2.36
RCA_2	Malyei (2)—beam	36	3.85
RCA_2	Malyei (2)—slab 1	37	4.15
RCA_5	Malyei (2)—slab 2	36	4.68

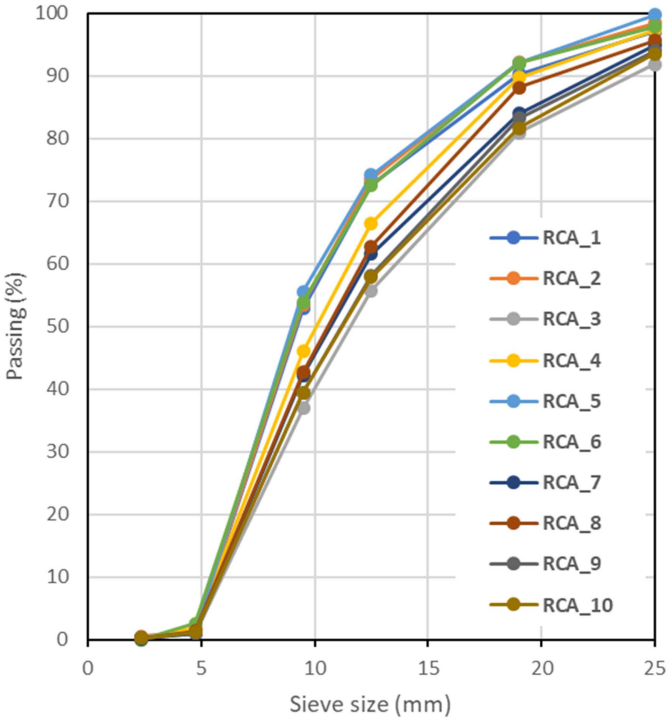

Fig. 6. Particle-size distribution of all RCA samples.

scope for interaction between particles, and providing a greater degree of compactness and mechanical strength (Kou and Poon 2008; Brand et al. 2015). The PSD of the RCA samples is summarized in Fig. 6. The results show that all samples followed the same pattern because they were crushed in the same jaw crusher, revealing that the various samples had comparable mechanical properties and can be combined to produce batches of aggregate. The percentage of the amounts in each fraction was similar, indicating that concrete prepared from this aggregate potentially will have positive performance.

Density. Bulk specific gravity typically has limited practical application in the formulation and production of concrete because it indicates only the density of the material that makes up the particles, which is a function of the original rock (Brand et al. 2015); however, the difference between specific gravity and the apparent specific gravity defines the water-retaining capacity of the particles. The recycled aggregate water absorption values varied between 5.2% and 8.5% (Table 5), and were similar to those obtained in other studies (Topçu and Şengel 2004). The residual mortar attached to the RCA is responsible for the higher water absorption capacity than of the NA, which was 2.11%.

Abrasion. The abrasion resistance test for coarse aggregate indicates the durability of an aggregate under dry conditions. Table 5 presents the Los Angeles abrasion values (corrosion ratio percentage) for all RCA samples, which were between 30% and 39%; the abrasion resistance value for the sample, including a mix of all RCA samples, was 6.30%. These results indicate that all the coarse aggregates complied with the maximum limit of corrosion ratio set in LNEC E 471:2009 (LNEC 2009) for use in structural concrete, which is 50%.

Chemical and Microstructural Properties of Coarse Aggregates

Chemical Analysis. The main chemical composition of the RCA samples collected from the 10 sites is presented in Table 6. Calcium oxide and silicon oxide were the main constituents, in varying quantities, and the high loss on ignition (LOI) indicates that the calcium was present at least in part as carbonates. These results indicate that the aggregate may come from two sources: quarries and rivers.

XRD Analysis. XRD was used to examine the mineralogical composition, and it was found that calcium carbonate (calcite) was the major crystalline compound in RCA_1 (Fig. 7), in addition to a small quantity of SiO_2 (quartz), and some minor portlandite. Fig. 8 shows the XRD results for all samples. Similar peaks of main phases were found for all RCA samples. The results collected from XRF and XRD analysis provide evidence that all samples had a similar composition. Hence, samples from different sites can be mixed and used to prepare new concretes, and can be considered as one sample.

TG-DTA Analysis. The RCA consisted of limestone or siliceous aggregates with old mortar adhered; therefore, its CaO and SiO_2 contents were not expected to be reactive (Anastasiou et al. 2018). Differential thermal analysis (DTA) and thermogravimetric analysis generally have been used to measure the main hydrated and carbonate phases in the samples (Rodrigues et al. 2013). The high value of loss on ignition can be attributed to the bonded water proportion and CO_2 quantity that was emitted from the sample (Anastasiou et al. 2018), and the DTA-TG results (Table 7 and Fig. 9) indicated a small amount of portlandite at 430°C–470°C and a high amount of $CaCO_3$ at 670°C–860°C.

Table 5. Specific gravity, apparent specific gravity, water absorption, and Los Angeles corrosion ratio of RCA samples

Sample ID	Oven dry bulk specific gravity (kg/m^3)	Apparent specific gravity (kg/m^3)	SSD bulk specific gravity (kg/m^3)	Water absorption (%)	Corrosion ratio (%)
RCA_1	2,296	2,599	2,413	5.1	30.7
RCA_2	2,196	2,512	2,322	5.7	32.7
RCA_3	2,144	2,557	2,305	7.5	39.0
RCA_4	2,210	2,535	2,338	5.8	30.1
RCA_5	2,222	2,558	2,353	5.9	36.9
RCA_6	2,078	2,513	2,251	8.3	34.9
RCA_7	2,185	2,574	2,336	6.9	37.4
RCA_8	2,085	2,482	2,245	7.7	34.5
RCA_9	2,151	2,515	2,296	6.7	32.8
RCA_10	2,125	2,473	2,266	6.6	38.1
NA (limestone)	1,673	1,863	1,775	2.1	31.5
RCA mix[a]	2,169	2,532	2,312	6.3	39.5

[a]RCA mix comprised a blend of RCA samples from all 10 sites identified in this study.

Table 6. Chemical compositions of NA (limestone) and RCAs determined by XRF (% by weight)

Compound	NA	RCA_1	RCA_2	RCA_3	RCA_4	RCA_5	RCA_6	RCA_7	RCA_8	RCA_9	RCA_10
CaO	56.4	48.7	42.6	52.1	46.4	46.9	49.8	50.3	52.9	50.6	51.4
SiO_2	1.6	11.7	21.0	7.0	14.4	12.1	9.0	9.2	5.0	8.1	6.6
Al_2O_3	0.4	2.0	3.7	1.2	2.6	2.4	1.8	1.9	1.1	1.8	1.6
Fe_2O_3	0.2	1.2	2.4	0.9	2.1	1.5	1.3	1.3	0.9	1.2	1.1
MgO	0.6	1.2	2.1	0.8	1.5	2.1	1.3	1.1	0.9	1.1	1.3
Na_2O	0.1	0.3	0.5	0.2	0.4	0.5	0.2	0.2	0.1	0.3	0.2
K2O	0.1	0.1	0.3	0.1	0.2	0.3	0.1	0.1	0.10	0.1	0.1
SO_3	0.0	0.5	1.0	0.4	0.6	0.7	0.6	0.5	0.4	0.5	0.4
TiO_2	0.1	0.2	0.3	0.2	0.2	0.2	0.2	0.2	0.2	0.2	0.2
P_2O_5	0.1	0.1	0.1	0.1	0.1	0.1	0.1	0.1	0.1	0.1	0.1
LOI	40.5	33.9	25.9	37.1	31.4	33.2	35.5	35.0	38.3	35.7	36.9

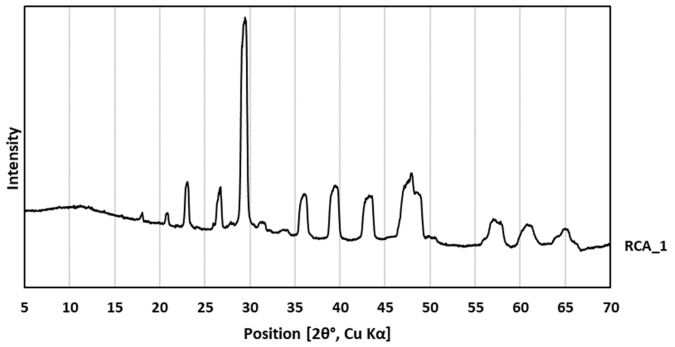

Fig. 7. XRD data for RCA_1.

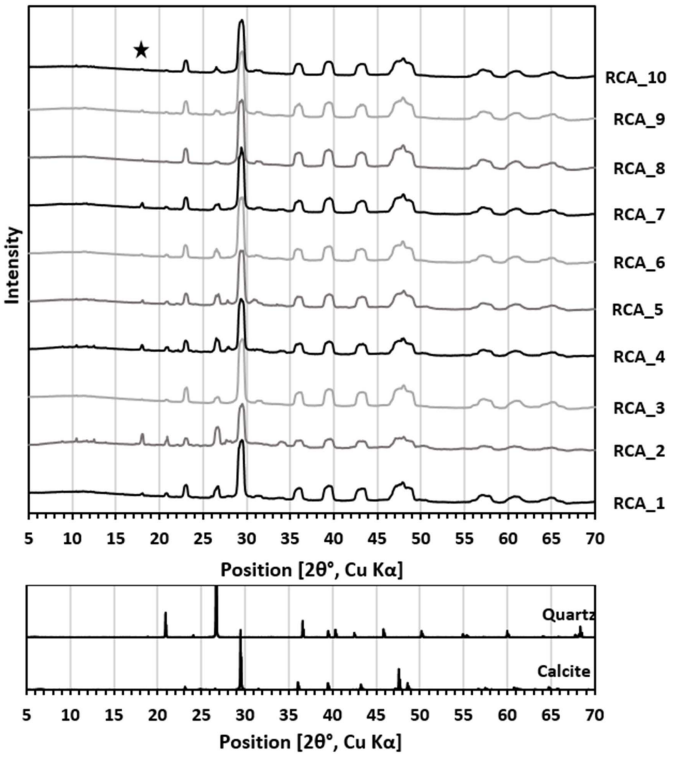

Fig. 8. XRD data for all RCA samples compared with reference patterns for quartz and for calcite. The star indicates the distinctive 001 peak of portlandite (18.09°2θ).

SEM Imaging. Fig. 10 gives an overview of the grain-size fractions 2–0.2 mm for two samples: one with calcareous RCA, and the other with silicate RCA. These micrographs show aggregates and mortars, as well as the cement matrix with finer particles, in which different phases can be determined by the grey level (Xie et al. 2015). Because porosity was the main focus here, only the porous area (Fig. 10, darkest area) was measured for the calculation of porosity.

The SEM images and EDX maps highlight the constituents of the two types of RCA; calcium and silicon are the main elements identified. In the third column in Fig. 10 the gray color refers to aggregate while the dark color related to mortar.

Workability and Density of Fresh Concrete

The results of the slump and density tests are summarized in Table 8. The slump values obtained for concrete class C25 were within the established limits of 100 ± 20 mm (Alexanderson 1971). The W/C ratio was adjusted to maintain the desired slump (Table 2).

Moreover, the percentage of RCA in the mixture influenced the concrete workability, so that the concrete with 75% and 100% of RCA had a higher W/C ratio than the other concretes, because the more porous RCA aggregate had a higher water demand than did natural aggregate in the mixture (Eguchi et al. 2007).

Table 9 presents the average bulk density of fresh concrete for each of the mixes. As expected, the density of the fresh concrete decreased as the content of RCA increased, which is justified by the presence of adhered old cement in RCA and the correspondingly lower density of this than of the natural aggregate (Table 5), as well as the higher water content of the RCA concretes.

Hardened Concrete Properties

Mechanical Properties

Compressive Strength. The 28-day compressive strength of the control mix was 41.5 MPa, whereas that for the RCA concrete mixes varied between 32.5 and 39.7 MPa (Fig. 11). The difference between the RCA0 and RCA25 samples was within the experimental error bounds, indicating that the effect of 25% RCA replacement on compressive strength was not statistically significant for the sample set tested here. The lowest value, 32.5 MPa, was 9 MPa less than that of the control mix; however, this value still was within the range of the established Syrian standards. The compressive strength of concrete is related to the hardness and strength of the aggregate particles; the cement mortar and the interfacial transition zone (ITZ) between the mortar and the aggregate is relatively weak, and the collapse in the concrete occurs at the weakest point (Scrivener et al. 2004). The recycled aggregate in the concrete was

Table 7. Quantification of TGA mass loss data for all samples, including assignment of mass loss events to temperature regions

Sample	H_2O 20°C–100°C	H_2O in C-S-H and other hydration products 105°C–430°C	H_2O in $Ca(OH)_2$ 430°C–470°C	CO_2 (physically and chemically bound) 250°C–925°C not otherwise accounted for	Total mass loss (%)	$Ca(OH)_2$ (%)	$CaCO_3$ (%)
RCA_1	0.76	1.90	0.33	34.88	37.11	3.12	79.28
RCA_3	0.59	1.41	0.30	38.07	40.37	2.44	86.52
RCA_4	0.99	2.47	0.49	31.27	34.22	4.05	71.06
RCA_5	0.89	2.20	0.35	33.49	36.04	3.65	76.12
RCA_6	0.90	2.20	0.32	35.42	37.95	3.70	80.51
RCA_7	1.01	2.46	0.47	33.23	36.16	4.16	75.53
RCA_8	0.65	1.46	0.22	39.10	40.77	2.68	88.86
RCA_9	0.89	1.99	0.29	35.98	38.26	3.65	81.78
RCA_10	0.79	1.72	0.25	37.31	39.28	3.23	84.79

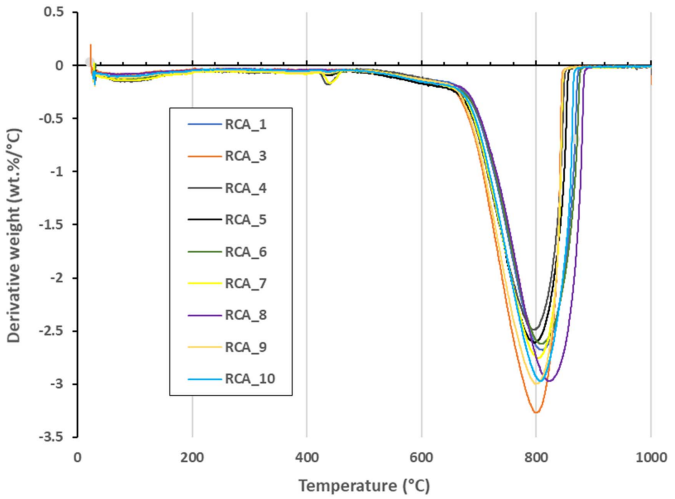

Fig. 9. DTA-TGA data for all recycled aggregate samples.

broken first during the application of compressive force to the concrete samples, as evident particularly in the fracture patterns visible on the left side of the sample in Fig. 12), which is related to the porosity of the adhered mortar on old aggregate grains, and the weakness of the new ITZ formed between the old mortar and new material (Dilbas et al. 2014).

Splitting Tensile Strength. The splitting tensile strength of the control mix (0% RCA) was slightly higher than that of the mixes containing RCA (Fig. 13), but the differences were not much greater than the experimental error bounds other than that for the 75% RCA sample. This means that the use of recycled coarse aggregate has no significant impact on the splitting tensile strength. Previous studies reported that the splitting tensile strengths of concretes containing 100% RCA consistently were 10% lower than that of conventional concrete (Matias et al. 2013) when comparing samples, and the results in Fig. 13 are consistent with that observation.

As the RCA percentage in the mixes increased, so did the splitting tensile strength–compressive strength ratios (Table 9). The improved ratio may be due to the presence of the attached

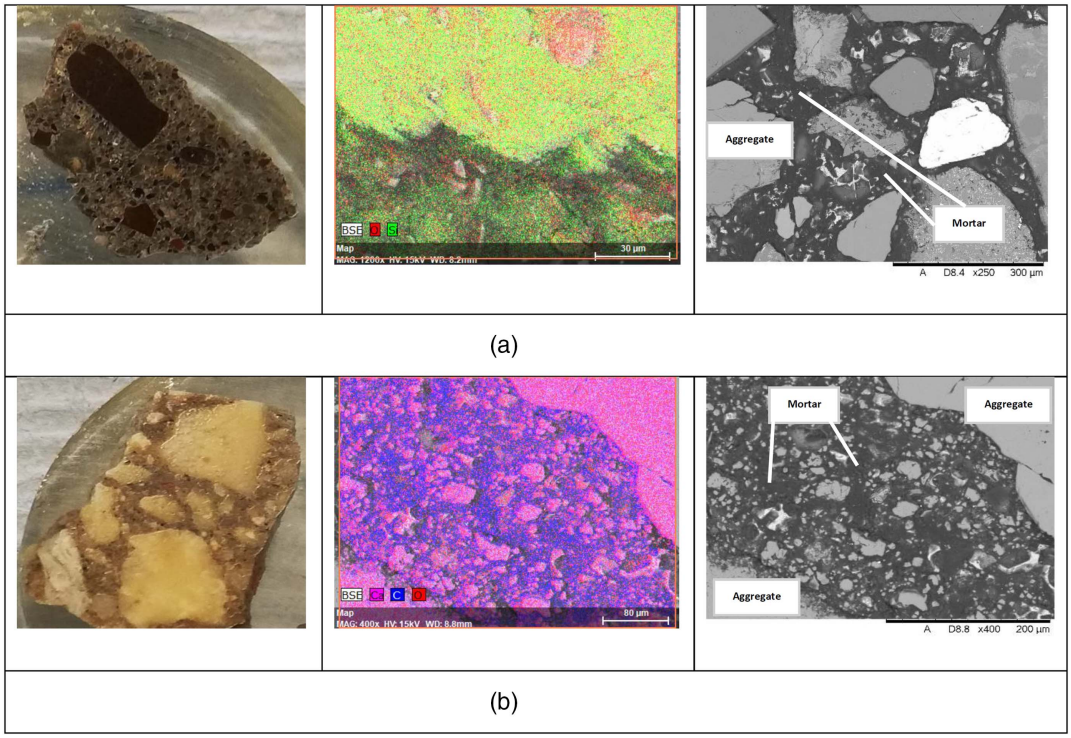

Fig. 10. Photographs and SEM images of selected RCA samples and corresponding EDS elemental maps: (a) silicate; and (b) calcareous.

Table 8. Properties of fresh concrete

Mix ID	Density (kg/m^3)	Slump (mm)
Control	2,330	90
RCA25	2,300	80
RCA50	2,240	80
RCA75	2,210	90
RCA100	2,190	80

Table 9. Summary of strength data, including calculated ratios of splitting tensile strength to compressive strength

Mix	RCA (% by weight)	Splitting tensile strength (MPa)	Compressive strength (MPa)	Ratio
Control	0	3.1	41.5	0.075
RCA25	25	3.1	39.7	0.078
RCA50	50	3.0	35.3	0.086
RCA75	75	2.8	32.5	0.086
RCA100	100	2.9	33.7	0.087

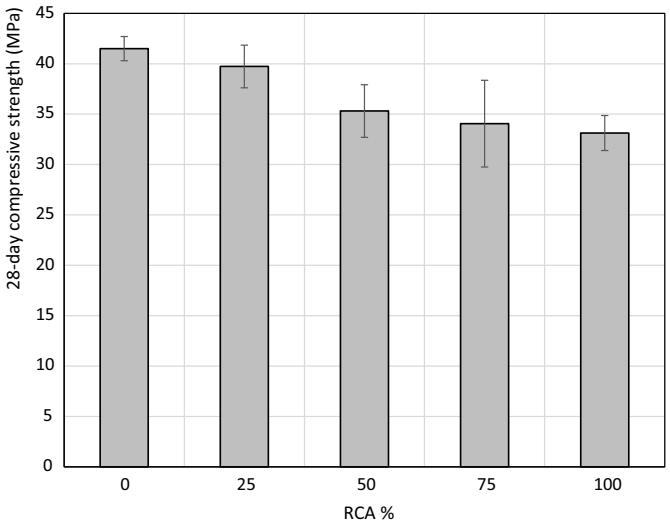

Fig. 11. Compressive strengths measured for all mixes.

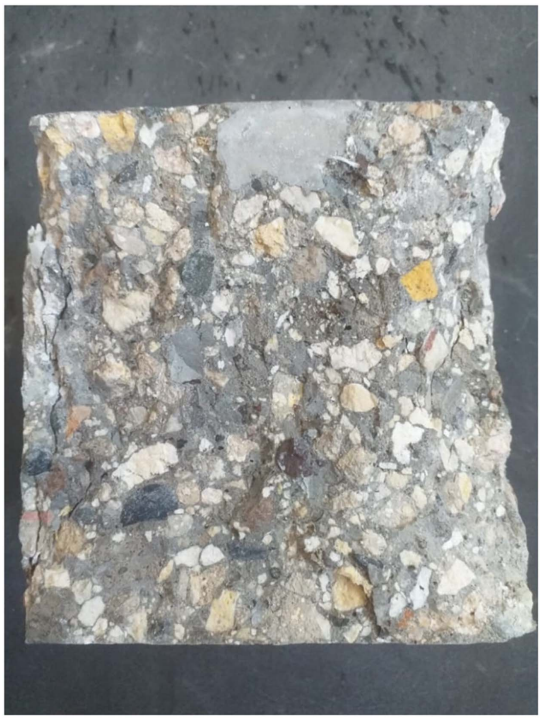

Fig. 12. Fracture surface of 100% RCA sample after compressive strength testing.

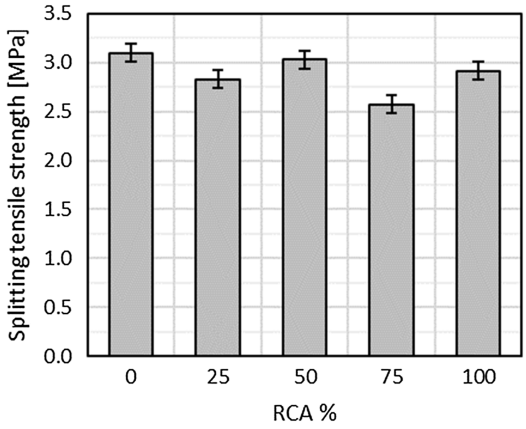

Fig. 13. Splitting tensile strengths measured for all mixes.

cement mortar, which would enhance the bonding between the RCA and the new cement paste (Sri Ravindrarajah and Tam 1985). Furthermore, the rough surface of the RCAs might peoduce additional interlocking effects in the microstructure of the ITZ (Kou and Poon 2008) and enhance the splitting tensile strength.

These results are consistent with the outcomes of some of the broader body of published research. For example, improvement of the tensile strength of RCA concrete has been observed when using saturated [~80% and 100% saturated surface dry (SSD)] aggregate (Brand et al. 2015). However, this behavior is not consistent across all published studies; other studies observed that regardless of the type of recycled aggregate used, the splitting tensile strength of the specimens before the age of 28 days decreased as a function of increasing RCA replacement ratio, although some increases were observed for 90-day-aged specimens (Kou et al. 2012). Thèrefore this remains an area requiring further research.

Flexural Strength. Flexural strength did not change considerably up to 50% RCA replacement; however, at higher replacement levels, flexural strength decreased (Fig. 14). As the percentage of RCA increases, the number and size of flexural cracks also increase, resulting in much higher deformations (Volz et al. 2014). The higher water content of the high-RCA mixes also may be relevant in controlling this behavior.

It has been found previously that the RCA replacement percentage has only a marginal influence on the flexural strength of recycled aggregate concrete (RAC) (Cheng 2005; Xiao and Li 2005). However, some authors found that as the RCA replacement increased, the flexural strength of RAC decreased (Topçu and Şengel 2004), whereas others concluded that no significant difference existed in the flexural strength of conventional concrete and RAC made with RCA (Sri Ravindrarajah and Tam 1985). The results presented here are aligned with the body of evidence available in the literature.

Elastic Modulus. The modulus of elasticity of concrete is highly dependent on the stiffnesses of the constituent phases (the aggregates, the cement paste regions, and the ITZ), as well as the

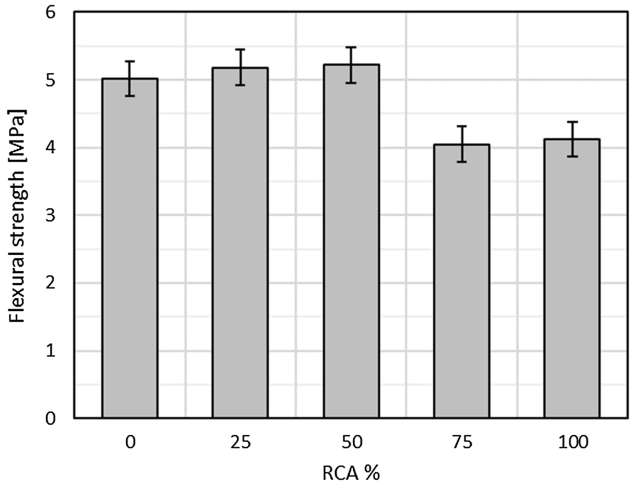

Fig. 14. Flexural strengths measured for all mixes.

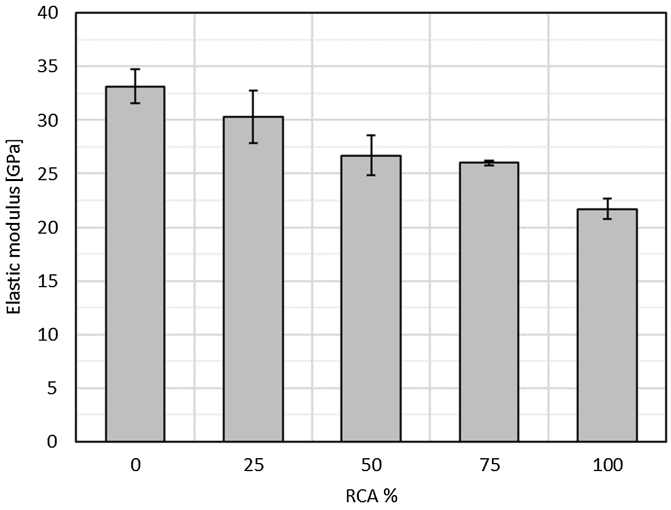

Fig. 15. Elastic modulus of all mixes.

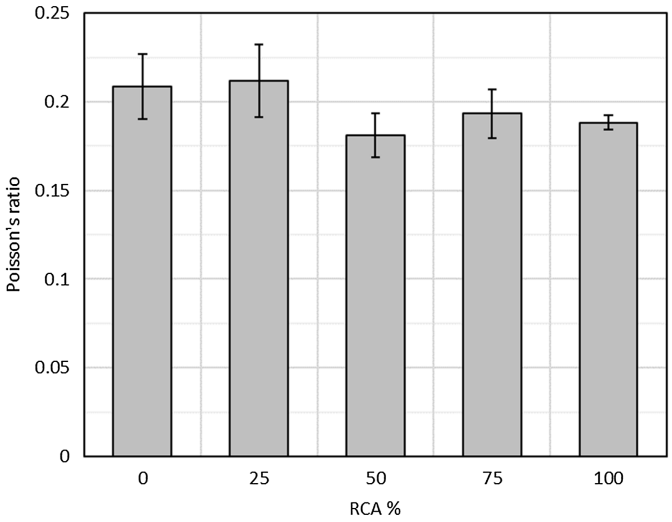

Fig. 16. Poisson's ratio of all mixes.

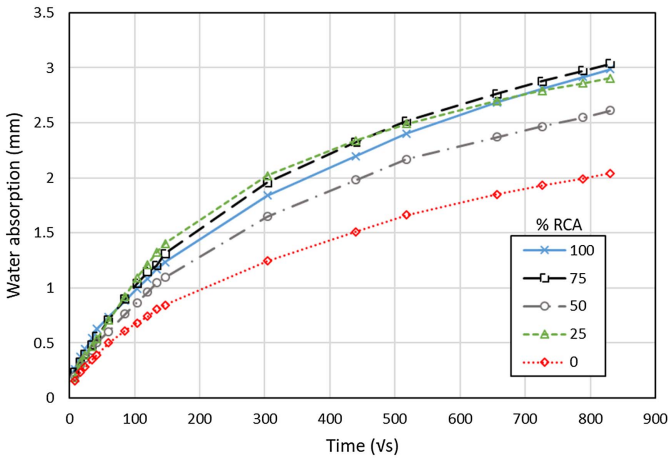

Fig. 17. Water absorption of all mixes.

presence of voids, defects, and cracks within the microstructure that incorporates these phases. Therefore, it is natural that as the replacement ratio of NA by RCA increases, the modulus of elasticity decreases.

Fig. 15 shows the modulus of elasticity of RAC as a function of the RCA percentage. The influence of RCA on the elastic modulus was significantly greater than on the compressive strength (Guo et al. 2018). The elastic modulus reduction ranged from 8.4% (25% RCA) to 34.1% (100% RCA) compared with the control concrete. This reduction was due to the lower stiffness and bulk density of RCA than of the NA (Huda and Alam 2014).

Concerning the values of the elastic modulus of RAC, many data reported in the literature show that if the virgin aggregate replacement percentage is as much as 100%, the elastic modulus is reduced by as much as 45% (Xiao et al. 2005). Topçu and Şengel (2004) found that the reduction of the elastic modulus of RAC was 80%, whereas Hansen and Boegh (1985) and Frondistou-Yannas (1977) reported that the reductions of the elastic modulus of RAC were 33% and 14%–28%, respectively. The main reason for these reported differences in the elastic modulus reduction is related to the different elastic moduli of RCA used by these different investigators. The fact that the RCA used here was derived from relatively good quality concrete meant that the reduction of elastic modulus was not as great as was reported by some other studies.

Poisson's Ratio. There was a slight reduction of Poisson's ratio with RCA replacement (Fig. 16). The Poisson's ratio decreased nearly 10% with 100% RCA in the concrete; this was the only measurement which was significantly different from the control when considering the experimental uncertainty. Although the value recorded for 50% RCA was lower than any others, this mix had a wider error bound in the measurements. Poisson's ratio plays a vital role in concrete structural performance (Bui et al. 2017), the expected range of values of Poisson's ratio for Portland cement concretes is 0.15–0.20 (Xiao et al. 2012a, b), and all of the values measured were within this range.

Water Absorption

The concrete mixes containing RCA all absorbed more water than the NA concrete, but there was not a monotonic increase in absorption with increasing RCA replacement level (Fig. 17). The absorption capacity of RCA is higher than that of NA due to the cement mortar attached to the aggregate particles (Xiao 2018). Incorporation of RCA results in more-numerous and longer capillaries and

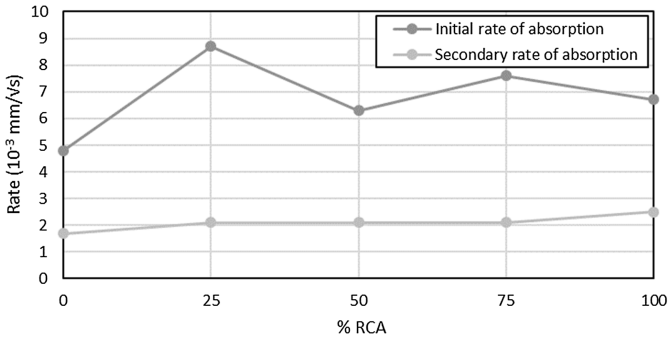

Fig. 18. Initial and secondary rates of absorption.

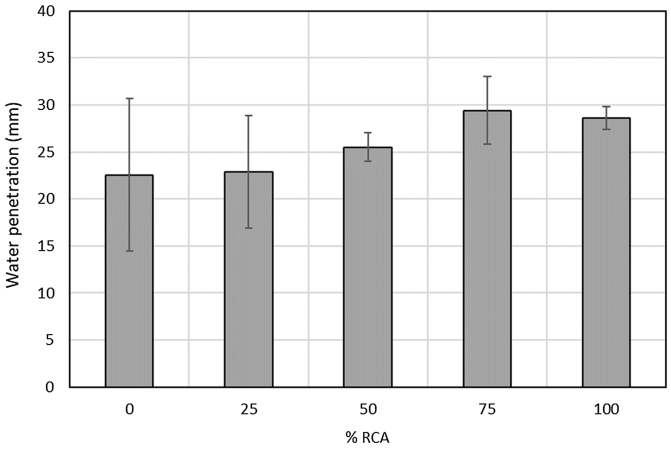

Fig. 20. Maximum water penetration depths.

a higher overall pore volume due to the higher porosity of RCA than NA, resulting in higher capillary forces (Wirquin et al. 2000; Evangelista and de Brito 2010). However, it appears that RCA contents higher than 50% do not cause consistent further changes in water absorption behavior; there were significant differences between the 0%, 25%, and 50% RCA mixes (the mechanical properties measurements of which all were more similar to each other, as wa discussed previously), but there was little difference between the 75% and 100% RCA mixes, although the mechanical properties of these differed more, e.g. flexural strength (Fig. 14).

Fig. 18 illustrates the water absorption rates of the samples for two periods: the initial rate (from 1 min to 6 h) and the secondary rate (from 1 day to 7 days). There was not a monotonic trend in the water absorption data in the early minutes of the test; the 25% RCA mix had the highest initial rate. However, the secondary rate increased consistently with RCA content. This is consistent with the literature, in which it was observed that with increasing RCA content, water absorption increases (Kurda et al. 2019), and the size of pores decreases over time due to the increased formation of hydration products in old mortar attached to RCA (Kurda et al. 2019). In the current set of samples, the effect of this difference in pore structure was reflected more clearly in the secondary rates than in the initial rates or total water uptake measurements.

Water Penetration

The water penetration fronts of all samples are marked with black lines in Fig. 19, and the results are summarized in Fig. 20. Concretes with RCA had a greater depth of water penetration than did the concrete with NA, which is consistent with previous studies (Kou et al. 2012). Under these conditions, it is confirmed that the differences observed between NA and RCA were due to the old mortar attached to the recycled aggregates, which absorbed more water. In general, a higher water penetration depth indicates a concrete with lower durability (Xiao and Li 2005).

Rapid Chloride Permeability Test (RCPT)

Fig. 21 shows the relationship between charge passed during the RCPT testing period and the percentage of RCA in concrete. The chloride penetration resistance of the 75% and 100% RCA

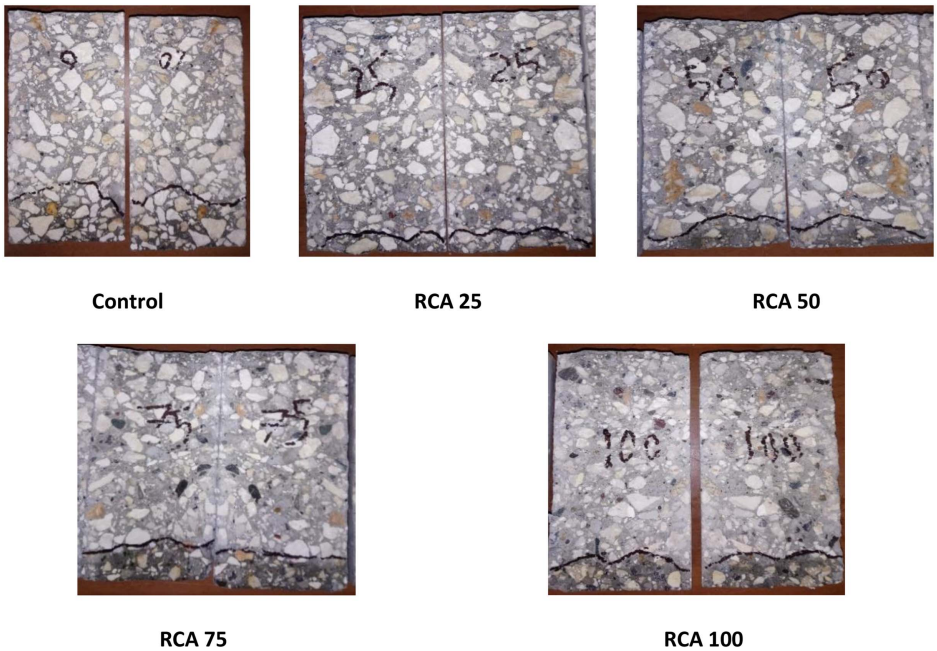

Fig. 19. Water permeability specimens showing visible water fronts.

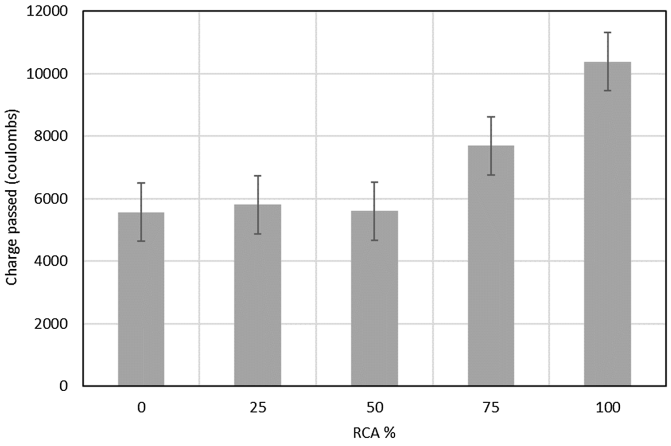

Fig. 21. Charge passed by all mixes during the RCPT test, as a measure of chloride penetrability.

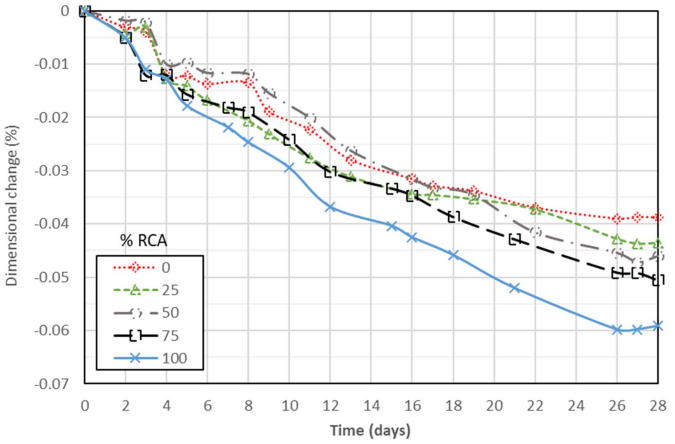

Fig. 22. Drying shrinkage of all mixes.

samples decreased (higher charge passed), whereas no significant increase of the chloride permeability was observed for the 25% or 50% RCA samples compared with the control mix. All specimens, including the control sample, had high chloride ion penetrability (>4,000 C) according to the classification of ASTM C1202.

The chloride penetration resistance of RCA concretes is known to decrease with increasing RCA content. Compared with a control mix, an increase of 15%–40% in the chloride permeability was observed previously for 100% RCA concrete (Thomas et al. 2018). The results of the present study are consistent with those findings. According to Wang et al. (2016), the porosity of the mortar phase determines the chloride penetration resistance in concrete, and the RCA was more porous than NA. Souche et al. (2017) proposed that another phenomenon that may increase the permeability of concrete is the release of absorbed water from within the aggregates to the cement paste, which increases the effective local W/C ratio. It is entirely possible that both of these mechanisms were involved in determining the performance of the samples studied here.

Volume of Permeable Pore Space

The volume of permeable pore space of the concrete samples is presented in Table 10. From 100% NA to 100% RCA, the volume of permeable pore spaces within the samples increased, largely due to the porosity within the RCA particles registering as pore space in the testing methods (and thus also reducing sample density), and also potentially in part due to the weaker bond involving the adhered old mortar in the RCA. The very marked increase in the volume of permeable voids from 50% to 100% RCA samples is well aligned with the trend in RCPT results (Fig. 23), but contrasts with the water absorption measurements (Fig. 20), in which there was little difference within this part of the sample set. There was not a clear relationship between the volume of permeable pore space and the mechanical properties (Figs. 11, 13, and 14); the 100% RCA sample was much more different from the other mixes in terms of porosity than it was in terms of compressive, tensile, or flexural strength.

Drying Shrinkage

Fig. 22 illustrates the effect of RCA content on the drying shrinkage of the concrete samples starting from 24 h to 28 days after casting. The trends were similar to the trends in RCPT results, because both of these material characteristics are fundamentally related to the volume of paste present in the samples. For concretes made with less RCA, lower shrinkage values were recorded in general. As expected, the drying shrinkage of concrete increased with the exposure time in all series. The drying shrinkage increase associated with the use of RAC was between 12% and 52% compared with that of conventional concrete at age 28 days. This may be because of the internal shrinkage of RAC (Mehta and Monteiro 2006), and/or the lower restraining capacity of RCA particles compared to natural aggregate (Sagoe-Crentsil et al. 2001), but it is very likely that there was an important influence from the higher water content of the RAC mixes here. Previous studies found the drying shrinkage of RAC to increase with increasing RCA replacement percentage and water–cement ratio (Zhu and Jin 2010), although others reported that it is possible to design high-quality RAC with shrinkage values close to that of conventional concrete (Zhang et al. 2009).

Recommendations for Using Syrian RCA and Potential Valorization Routes for Rubble

As of November 2018, the total number of detected damaged structures in affected areas of Syria was 131,426, and 70% of

Table 10. Water absorption of concretes with RCA at each stage within ASTM C642 determination of volume of permeable pores

Mix	Absorption after immersion (%)	Absorption after immersion and boiling (%)	Bulk density dry (kg/m^3)	Bulk density after immersion (kg/m^3)	Bulk density after immersion and boiling (kg/m^3)	Apparent density (kg/m^3)	Volume of permeable pore space (%)
Control	5.82	6.82	2,183	2,310	2,332	2,565	14.9
RCA25	6.55	7.41	2,159	2,300	2,319	2,570	16.0
RCA50	6.57	7.35	2,125	2,265	2,282	2,519	15.6
RCA75	7.89	7.67	2,124	2,291	2,287	2,537	16.3
RCA100	9.11	9.92	2,010	2,193	2,209	2,510	19.9

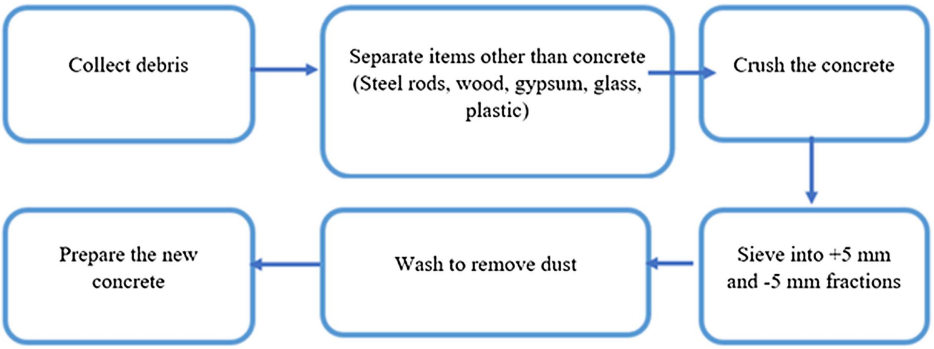

Fig. 23. Proposed procedure for recovery of debris into valuable RCA for reconstruction in Syria.

the structural material in these was concrete (REACH 2019). A residential building consisting of four floors, with an area of 100 m^2, contains about 165 m^3 of RC, and the weight of the concrete is approximately 420 t (Syrian Engineers Union 2006). Therefore, this quantity of approximately 38.5 million t of crushed concrete is an important alternative to the natural aggregates used in Syria's concrete industry because urgent reconstruction efforts are needed. This quantity of material also is a tremendous burden on the environment unless it is disposed of. Fig. 23 presents one of the strategies suggested in this context.

The technical results presented in this paper provide essential support for the capability to use postconflict debris in Syria as recycled aggregate in concretes, ensuring that the concretes produced in this way for civil and infrastructure reconstruction can meet the required quality standards. It is imperative that reconstruction efforts are completed with high quality and using materials that are technically sound, durable, and reliable, because the citizens returning to damaged areas must be able to have full confidence in the safety and future serviceability of the infrastructure that is rebuilt for them. Therefore the procedure in Fig. 23 should be used as a guideline to ensure that Syria's reconstruction is successful, environmentally responsible, and as rapid as possible for the benefit of the displaced citizens.

Conclusions

From the present study, the following conclusions have been reached:

- Aggregate samples collected from different sites in Syria exhibit more-or-less similar properties, and the main minerals in the samples were calcite and quartz. For this reason, the recovered materials can be mixed together to prepare new concretes.
- Compared with NA, RCA has high water absorption and low apparent density due to the adhered old mortar in the RCA, which might create workability issues. To solve this problem, RCA could be soaked with water for 24 h before being used in new concrete production.
- Mechanical properties such as compressive, splitting, and flexural strength and elastic modulus decreased because of the weakness of both the old interfacial transition zone within the RCA and the new interfacial transition zone between the old and new mortars. Up to 50% replacement of NA with RCA in new concrete conforms to Syrian standard grade C20, which is used in a wide range of construction elements.
- The durability of new concretes made with RCA replacement levels up to 50% also slightly decreased, because the porosity of old mortar allowed water and chloride to penetrate more easily. These potentially could be avoided through pretreatment of the RCA or utilization of supplementary cementitious materials or admixtures that can be used in addition to the raw materials in concrete mixture designs.

Data Availability Statement

All data, models, and code generated or used during the study appear in the published article.

Acknowledgments

We thank CARA (https://www.cara.ngo/) because this work would not have been possible without their financial support, and the input of Kate Robertson (CARA) and Dr. David Read (University of Sheffield) in particular. We are especially indebted to Dr. Oday Hussein, Dr. Sarah Kearney, Dr. Daniel Geddes, Chun Long Woo, Dr. Martin Stennett, and Dr. Nik Reeves-McLaren from the Department of Materials Science and Engineering, University of Sheffield, who conducted many mineralogical tests. We are grateful to students from Sham University who helped us in collecting RCA samples: Ibrahim Al sheikh Saleh, Mohamed Al-Khateeb, and Said Othman. Sample collection was conducted under the University of Sheffield ethics approval Reference 024525.

References

Alexanderson, J. 1971. "Design of concrete mixes." *Matériaux et Constr./ Mater. Struct.* 4 (4): 203–212. https://doi.org/10.1007/BF02478946.

Anastasiou, E., M. Papachristoforou, D. Anesiadis, K. Zafeiridis, and E.-C. Tsardaka. 2018. "Investigation of the use of recycled concrete aggregates originating from a single ready-mix concrete plant." *Appl. Sci.* 8 (11): 2149. https://doi.org/10.3390/app8112149.

ASTM International. 1997. *Standard test method for density, absorption, and voids in hardened concrete*. ASTM C642-97. West Conshohocken, PA: ASTM.

ASTM International. 2001a. *Standard test method for density (unit weight), yield, and air content (gravimetric)*. ASTM C138/C138M-01a. West Conshohocken, PA: ASTM.

ASTM International. 2001b. *Standard test method for sieve analysis of fine and coarse aggregates*. ASTM C136-01. West Conshohocken, PA: ASTM.

ASTM International. 2001c. *Standard test method for specific gravity and water absorption of coarse aggregate*. ASTM C127-01. West Conshohocken, PA: ASTM.

ASTM International. 2002a. *Standard test method for flexural strength of concrete (using simple beam with third-point loading)*. ASTM C293-02. West Conshohocken, PA: ASTM.

ASTM International. 2002b. *Standard test method for splitting tensile strength of cylindrical concrete*. ASTM C496/C496M-02. West Conshohocken, PA: ASTM.

ASTM International. 2002c. *Standard test method for static modulus of elasticity and poisson's ratio of concrete*. ASTM C469-02. West Conshohocken, PA: ASTM.

ASTM International. 2003a. *Standard test method for resistance to degradation of small-size coarse aggregate by abrasion and impact in the Los Angeles machine*. ASTM C131-03. West Conshohocken, PA: ASTM.

ASTM International. 2003b. *Standard test method for slump of hydraulic-cement concrete.* ASTM C143/C143M-03. West Conshohocken, PA: ASTM.

ASTM International. 2012. *Standard test method for electrical indication of concrete's ability to resist chloride ion penetration*. ASTM C1202. West Conshohocken, PA: ASTM.

ASTM International. 2013. *Standard test method for measurement of rate of absorption of water by hydraulic cement concretes*. ASTM C1585-13. West Conshohocken, PA: ASTM.

ASTM International. 2018a. *Standard test method for compressive strength of cylindrical concrete specimens*. ASTM C39/C39M-18. West Conshohocken, PA: ASTM.

ASTM International. 2018b. *Standard test method for rebound number of hardened concrete*. ASTM C805/C805M-1. West Conshohocken, PA: ASTM.

Brand, A. S., J. R. Roesler, and A. Salas. 2015. "Initial moisture and mixing effects on higher quality recycled coarse aggregate concrete." *Constr. Build. Mater.* 79 (Mar): 83–89. https://doi.org/10.1016/j.conbuildmat.2015.01.047.

BSI (British Standards Institution). 2003. *Depth of penetration of water under pressure*. BS EN 12390-8:2000. London: BSI.

Bui, N. K., T. Satomi, and H. Takahashi. 2017. "Improvement of mechanical properties of recycled aggregate concrete basing on a new combination method between recycled aggregate and natural aggregate." *Constr. Build. Mater.* 148 (Sep): 376–385. https://doi.org/10.1016/j.conbuildmat.2017.05.084.

CEN (European Committee for Standardization). 2011. *Cement–Composition, specifications and conformity criteria for common cements*. EN 197-1:2011. Brussels, Belgium: CEN.

CEN (European Committee for Standardization). 2013. *Aggregates for concrete*. EN 12620:2013. Brussels, Belgium: CEN.

CEN (European Committee for Standardization). 2016. *Concrete. Specification, performance, production and conformity.* EN 206:2013 +A1:2016. Brussels, Belgium: CEN.

Cheng, G.-Y. 2005. "Experimental study on the basic performance of recycled aggregate concrete with different displacement ratio." *Chin. Concr. J.* 11: 67–70.

Cheung, F., A. Kube, L. Tay, E. Diener, J. J. Jackson, R. E. Lucas, M. Y. Ni, and G. M. Leung. 2020. "The impact of the Syrian conflict on population well-being." *Nat. Commun.* 11 (1): 3899. https://doi.org/10.1038/s41467-020-17369-0.

Dilbas, H., M. Şimşek, and Ö. Çakır. 2014. "An investigation on mechnical and physical properties of recycled aggregate concrete (RAC) with and without silica fume." *Constr. Build. Mater.* 61 (Jun): 50–59. https://doi.org/10.1016/j.conbuildmat.2014.02.057.

Eguchi, K., K. Teranishi, A. Nakagome, H. Kishimoto, K. Shinozaki, and M. Narikawa. 2007. "Application of recycled coarse aggregate by mixture to concrete construction." *Constr. Build. Mater.* 21 (7): 1542–1551. https://doi.org/10.1016/j.conbuildmat.2005.12.023.

Evangelista, L., and J. de Brito. 2010. "Durability performance of concrete made with fine recycled concrete aggregates." *Cem. Concr. Compos.* 32 (1): 9–14. https://doi.org/10.1016/j.cemconcomp.2009.09.005.

Frondistou-Yannas, S. 1977. "Waste concrete as aggregate for new concrete." *ACI J. Proc.* 78 (8): 373–376.

Guo, H., C. Shi, X. Guan, J. Zhu, Y. Ding, T.-C. Ling, H. Zhang, and Y. Wang. 2018. "Durability of recycled aggregate concrete—A review." *Cem. Concr. Compos.* 89 (May): 251–259. https://doi.org/10.1016/j.cemconcomp.2018.03.008.

Hansen, T. C., and E. Boegh. 1985. "Elasticity and drying shrinkage of recycled-aggregate concrete." *ACI J. Proc.* 82 (5): 648–652.

Huda, S. B., and M. S. Alam. 2014. "Mechanical behavior of three generations of 100% repeated recycled coarse aggregate concrete." *Constr. Build. Mater.* 65 (Aug): 574–582. https://doi.org/10.1016/j.conbuildmat.2014.05.010.

ISO. 2009. *Testing of concrete—Part 8: Determination of drying shrinkage of concrete for samples prepared in the field or in the laboratory.* ISO 1920-8:2009. Geneva: ISO.

Kou, S.-C., and C.-S. Poon. 2008. "Mechanical properties of 5-year-old concrete prepared with recycled aggregates obtained from three different sources." *Mag. Concr. Res.* 60 (1): 57–64. https://doi.org/10.1680/macr.2007.00052.

Kou, S.-C., C.-S. Poon, and H.-W. Wan. 2012. "Properties of concrete prepared with low-grade recycled aggregates." *Constr. Build. Mater.* 36 (Nov): 881–889. https://doi.org/10.1016/j.conbuildmat.2012.06.060.

Kurda, R., J. de Brito, and J. D. Silvestre. 2019. "Water absorption and electrical resistivity of concrete with recycled concrete aggregates and fly ash." *Cem. Concr. Compos.* 95 (Jan): 169–182. https://doi.org/10.1016/j.cemconcomp.2018.10.004.

Limbachiya, M. C., T. Leelawat, and R. K. Dhir. 2000. "Use of recycled concrete aggregate in high-strength concrete." *Mater. Struct.* 33 (9): 574–580. https://doi.org/10.1007/BF02480538.

LNEC (Laboratório Nacional de Engenharia Civil). 2009. *Guia para a utilização de agregados reciclados em camadas não ligadas de pavimentos*. LNEC E473-2009. Lisbon, Portugal: LNEC.

Matias, D., J. de Brito, A. Rosa, and D. Pedro. 2013. "Mechanical properties of concrete produced with recycled coarse aggregates—Influence of the use of superplasticizers." *Constr. Build. Mater.* 44 (Jul): 101–109. https://doi.org/10.1016/j.conbuildmat.2013.03.011.

Mehta, P. K., and P. J. M. Monteiro. 2006. *Concrete: Microstructure, properties, and materials*. 3rd ed. New York: McGraw-Hill.

Qudsi, J. 2017. *Rebuilding old Aleppo—Postwar sustainable recovery and urban refugee resettlement*. New York: New York Univ.

REACH. 2019. "Syrian cities damage atlas." Accessed September 22, 2021. https://reliefweb.int/sites/reliefweb.int/files/resources/reach_thematic_assessment_syrian_cities_damage_atlas_march_2019_reduced_file_size_1.pdf.

Rodrigues, F., M. T. Carvalho, L. Evangelista, and J. de Brito. 2013. "Physical–chemical and mineralogical characterization of fine aggregates from construction and demolition waste recycling plants." *J. Cleaner Prod.* 52 (Aug): 438–445. https://doi.org/10.1016/j.jclepro.2013.02.023.

Sagoe-Crentsil, K. K., T. Brown, and A. H. Taylor. 2001. "Performance of concrete made with commercially produced coarse recycled concrete aggregate." *Cem. Concr. Res.* 31 (5): 707–712. https://doi.org/10.1016/S0008-8846(00)00476-2.

Scrivener, K. L., A. K. Crumbie, and P. Laugesen. 2004. "The interfacial transition zone (ITZ) between cement paste and aggregate in concrete." *Interface Sci.* 12 (4): 411–421. https://doi.org/10.1023/B:INTS.0000042339.92990.4c.

Souche, J.-C., P. Devillers, M. Salgues, and E. Garcia Diaz. 2017. "Influence of recycled coarse aggregates on permeability of fresh concrete." *Cem. Concr. Compos.* 83 (Oct): 394–404. https://doi.org/10.1016/j.cemconcomp.2017.08.002.

Sri Ravindrarajah, R., and C. T. Tam. 1985. "Properties of concrete made with crushed concrete as coarse aggregate." *Mag. Concr. Res.* 37 (130): 29–38. https://doi.org/10.1680/macr.1985.37.130.29.

Syrian Engineers Union. 2006. *Appendix 1 for the Syrian Arab code for the design and implementation of reinforced concrete structures-loads on buildings*. Damascus, Syria: Syrian Engineers Union.

Teychenné, D. C., R. E. Franklin, and H. C. Erntroy. 1997. *Design of normal concrete mixes*. BR331. 2nd ed. Bracknell, UK: IHS BRE Press.

Thomas, J., N. N. Thaickavil, and P. M. Wilson. 2018. "Strength and durability of concrete containing recycled concrete aggregates." *J. Build. Eng.* 19 (Sep): 349–365. https://doi.org/10.1016/j.jobe.2018.05.007.

Topçu, I. B., and S. Şengel. 2004. "Properties of concretes produced with waste concrete aggregate." *Cem. Concr. Res.* 34 (8): 1307–1312. https://doi.org/10.1016/j.cemconres.2003.12.019.

Volz, J., K. H. Khayat, M. Arezoumandi, J. Drury, S. Sadati, A. Smith, and A. Steele. 2014. *Recycled concrete aggregate (RCA) for infrastructure elements*. Rep. No. cmr14-014. Jefferson City, MO: Missouri DOT.

Wang, H., X. Sun, J. Wang, and P. J. M. Monteiro. 2016. "Permeability of concrete with recycled concrete aggregate and pozzolanic materials under stress." *Materials* 9 (4): 252. https://doi.org/10.3390/ma9040252.

Wirquin, E., R. Hadjieva-Zaharieva, and F. Buyle-Bodin. 2000. "Utilisation de l'absorption d'eau des bétons comme critères de leur durabilité—Application aux bétons de granulats recycles. [Use of water absorption by concrete as a criterion of the durability of concrete-application to recycled aggregate concrete.]" *Mater. Struct.* 33 (6): 403–408. https://doi.org/10.1007/BF02479650.

Xiao, J. 2018. *Recycled aggregate concrete structures*. Berlin: Springer. https://doi.org/10.1007/978-3-662-53987-3.

Xiao, J., J. Li, and C. Zhang. 2005. "Mechanical properties of recycled aggregate concrete under uniaxial loading." *Cem. Concr. Res.* 35 (6): 1187–1194. https://doi.org/10.1016/j.cemconres.2004.09.020.

Xiao, J., W. Li, Y. Fan, and X. Huang. 2012a. "An overview of study on recycled aggregate concrete in China (1996-2011)." *Constr. Build. Mater.* 31 (Jun): 364–383. https://doi.org/10.1016/j.conbuildmat.2011.12.074.

Xiao, J., W. Li, and C. Poon. 2012b. "Recent studies on mechanical properties of recycled aggregate concrete in China—A review." *Sci. China Technol. Sci.* 55 (6): 1463–1480. https://doi.org/10.1007/s11431-012-4786-9.

Xiao, J.-Z., and J. Li. 2005. "Study on relationships between strength indexes of recycled concrete." *J. Build. Mater.* 8 (2): 197–201.

Xie, Y., D. J. Corr, F. Jin, H. Zhou, and S. P. Shah. 2015. "Experimental study of the interfacial transition zone (ITZ) of model rock-filled concrete (RFC)." *Cem. Concr. Compos.* 55 (Jan): 223–231. https://doi.org/10.1016/j.cemconcomp.2014.09.002.

Zhang, J., H. Du, C. Zhang, and Q. Li. 2009. "Influence of mineral admixture and recycled aggregate on shrinkage of concrete." *J. Qingdao Technol. Univ.* 34 (4): 145–149.

Zhu, L., and W. Jin. 2010. "The study on early drying shrinkage of recycled aggregate concrete." In *Proc., 2nd Int. Conf. on Waste Engineering and Management—ICWEM 2010*, 568–575. Paris, France: RILEM.